Influence of the shape on the roughness-induced transition

J.-Ch. Loiseau, S. Cherubini, J.-Ch. Robinet, E. Leriche

Abstract Global instability analysis of the three-dimensional flow past two roughness elements of different shape, namely a cylinder and a bump, is presented. In both cases, the eigenspectrum is made of modes characterised by a varicose symmetry and localised mostly in the zones of large base flow shear. The primary instability exhibited is the same in both cases and consists in an isolated unstable mode closely related to streaks local instability. For the cylinder however, a whole branch of modes is in addition destabilised as the Reynolds number is further increased.

1 Introduction

Delaying transition in spatially developing boundary layer flows has been a long time challenge. For small amplitude disturbances and supercritical Reynolds numbers, the linear stability theory predicts the slow transition process due to the generation, amplification and secondary instability of Tollmien-Schlichting (TS) waves. It has been shown recently in Ref.[1] that those TS waves can be stabilised by streamwise streaks. In this experimental work, sub-optimal streaks have been created using a periodic array of cylindrical roughness elements. Despite the stabilising effect of the streaks on the TS waves, the flow may undergo transition to turbulence right

J.-Ch. Loiseau
Laboratoire DynFluid, Arts et Métiers ParisTech, 151, Bd. de l'Hopital, 75013 Paris, France, e-mail: loiseau.jc@gmail.com

S. Cherubini
Laboratoire DynFluid, Arts et Métiers ParisTech, 151, Bd. de l'Hopital, 75013 Paris, France

J.-Ch. Robinet
Laboratoire DynFluid, Arts et Métiers ParisTech, 151, Bd. de l'Hopital, 75013 Paris, France

E. Leriche
Laboratoire de Mécanique de Lille, Université Lille-1, Boulevard Paul Langevin 59655 Villeneuve d'Ascq, FRANCE

downstream the roughness elements provided the streaks are strong enough. This roughness-induced transition has been extensively investigated experimentally by different authors [2, 3, 4]. For cylindrical roughness elements, in the early 60's, most of the results available back then have been reviewed in Ref.[5] into one transition diagram, thus giving an empirical criterion for transition. However, fewer studies have been carried out on smooth roughness elements, and the influence of the shape of the roughness on the destabilisation process has not yet been investigated in detail. Though the mechanism responsible for transition to turbulence in the flow past a 3D roughness element is not yet fully understood, it is believed that it is due to an instability of the streaks induced by the roughness elements. Thus, in order to investigate the origin of unsteadiness, a global instability analysis on the three-dimensional flow past a sharp-edged and a smooth roughness element is performed.

2 Problem formulation

The aim of the present work is to investigate the influence of the shape of the roughness element on the streaks generation further downstream along with their possible global instability. Two different kinds of roughness elements having aspect ratio $d/k = 2$ (where d is the diameter and k is the maximum height of the roughness), both mounted on a flat plate, have thus been considered: a cylindrical roughness element, and a smoother one defined by a cubic cosine function, $h(r) = k\cos^3(\pi r/d)$, r being the distance from the centre of the bump on the $x-z$ plane.
The flow past these roughness elements is studied using the 3D incompressible Navier-Stokes (NS) equations, non-dimensionalised with respect to the maximum height k of the roughness and the free-stream velocity U_∞; therefore, the Reynolds number is defined as $Re = U_\infty k/\nu$, ν being the kinematic viscosity. The computational domain extends from $x = -15$ to $x = 90$ in the streamwise direction, has a spanwise extent of $L_z = 16$ and wall-normal dimension $L_y = 50$ such that the global stability results are almost independent of the domain size. The Blasius velocity profile prescribed at the inlet ($x = -15$) is chosen such that, in the absence of the roughness element, one would have a theoretical Blasius boundary layer thickness of $\delta_{99} = 2$ at $x = 0$.
The behaviour of an infinitesimal perturbation $\mathbf{q} = (\mathbf{u}, p)^T$ superposed to a 3D steady state $\mathbf{Q} = (\mathbf{U}, P)^T$ has been studied using a global stability analysis. The steady base flows have been computed using the selective frequency damping (SFD) approach introduced in Ref.[6]. The following boundary conditions have been applied: at the inlet, the Blasius boundary layer velocity profile is imposed for the streamwise and wall-normal components of the velocity, whereas its spanwise component is set to zero. At the outlet, a standard outflow boundary condition is used. In the spanwise direction, periodic boundary conditions are imposed for the three components of the velocity. At the upper boundary, the streamwise component has been set equal to U_∞, and a Neumann condition on the wall-normal direction has been

imposed for the wall-normal and spanwise components of the velocity. Finally, a no-slip condition is imposed on the flat plate and the roughness element's walls.
Once the base flow has been computed, the NS equations are linearised around such a steady state, leading to a problem of the following type:

$$\frac{\partial \mathbf{u}}{\partial t} = A\mathbf{u}, \tag{1}$$

which is subject to the same boundary conditions as previously except regarding the inflow and the upper boundaries where a zero-velocity condition is prescribed. To perform a global stability analysis, one has to compute the eigenvalues of the Jacobian matrix A, which is a hard computational task due to the large number of degrees of freedom involved. Thus, a time-stepper approach as introduced in Ref.[7] and Ref.[8] has been used, which avoids the explicit storage of A and direct computation of its eigenvalues.
All of the calculations were performed using the code Nek5000 [9]. Spatial discretisation is done by a spectral elements method with Lagrange polynomials of order $N = 8$. The convective terms are advanced in time using an extrapolation of order 3, whereas the viscous terms use a backward differentiation of order 3 as well.

3 Results and discussion

Figure 1 shows base flows obtained at $Re = 1000$ for both roughness elements considered. An upstream and a downstream reversed flow region are shown in the right frames of figure 1 by the $U = 0$ isosurface (blue). In the left frames, the streaks induced by the roughness elements, being defined as the deviation of the base flows from the Blasius velocity profile U_B as in Ref.[4], are plotted. These flows share similar features: five streaks can be observed, two positive (red) and three negative (green) ones. These are induced by the presence of strong horseshoe vortices wrapped around the roughness elements, whose legs transport the low and high-momentum flow upwards and downwards in the boundary layer. These counter-rotating vortices induce the two outer pairs of streaks, whereas the central low-speed one is due to the streamwise velocity deficit induced by the roughness element.
Though their main structure is similar, some differences are found between the two flow fields. Indeed, for the case of the bump: (i) the separation zone is smaller than for the cylinder; (ii) the horseshoe vortex wrapping around the roughness element is much more spanwise-localised, its legs being weaker and closer one to the other; (iii) the streaks are weaker and quickly fade away downstream of the roughness element, whereas for the cylinder they appear to sustain on a much longer streamwise extent.

The eigenspectra obtained for the cylinder case at $Re = 800$ and $Re = 1000$ are provided in Figure 2 (a) and (b), respectively. At $Re = 800$, one can observe a single isolated eigenvalue lying almost on the neutral axis. Slightly increasing the Reynolds number drives the most unstable mode to move towards the upper-half

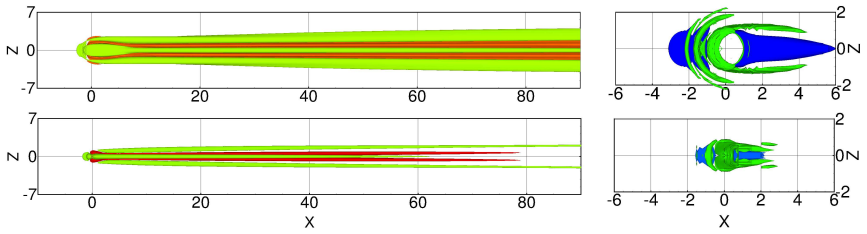

Fig. 1 Base flows computed at $Re = 1000$ in the presence of a cylinder (top) and a bump (bottom). The left frames show positive (red) and negative (green) surfaces of $U_{st} = U - U_B$, with $U_{st} = \pm 0.1$ (top) and $U_{st} = \pm 0.05$ (bottom); the right frames show isosurfaces of the $U = 0$ contour (blue), highlighting the separation zone, and the Q-criterion (green, for $Q = 0.1$).

complex plane, so that the flow becomes globally unstable at $Re_{cr} \approx 805$. Further increasing the Reynolds number yields a whole branch of eigenvalues to move in the upper-half complex plane, as shown in Figure 2 (b) for $Re = 1000$.
Regarding the bump, a similar behaviour has been found. Figure 2 (c) shows the eigenspectrum obtained for $Re = 800$. As previously, a single isolated mode is observed within the lower-half complex plane. When the Reynolds number is increased this eigenvalue moves upwards, reaching the upper-half of the complex plane at $Re_{cr} \approx 891$ as shown on figure 2 (d).

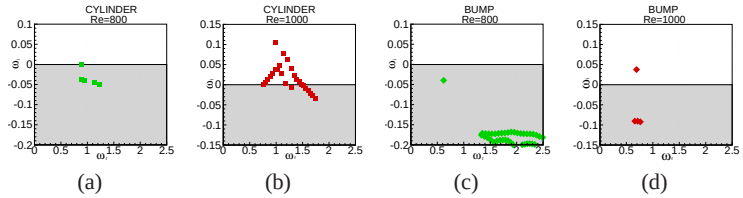

Fig. 2 Eigenspectra obtained for the flow past a cylinder with $Re = 800$ (a) and $Re = 1000$ (b), and for the flow past a bump with $Re = 800$ (c) and $Re = 1000$ (d).

As to get some insights on the instability mechanisms, the shape of the two unstable global modes is closely looked at. Figure 3 provides the streamwise component of the velocity for the most unstable eigenmode obtained at $Re = 1000$ for the cylinder case (left) and the bump one (right). These global modes are both characterised by streamwise alternated patches of positive/negative velocity developing mostly along the central low-speed streak, showing a symmetry with respect to the $z = 0$ plane. For the cylindrical element, the wave packet is placed well downstream of the roughness element, in a region where the streaks are well-developed and quasi-parallel. On the other hand, in the bump case, the most unstable eigenmode is placed closer to the roughness element which is concordant with the weaker streaks and gradients induced by the bump as well as their smaller streamwise extent.
The location and structure of the spatial support of the most unstable modes with

respect to the base flow streaks at $Re = 1000$ are shown in figure 4 (a) and (b) for both cases, respectively. For the cylinder case, the streamwise velocity contours of the eigenvector (shaded contours) and of the base flow (solid lines) are provided in the $x = 25$ plane. The strong deformation of the $U = const$ contours indicates the large amplitude of the streaks. The zones of maximum amplitude of the eigenvector are localised on the flanks and the top of the streaks, where the spanwise and wall-normal shears are the largest. A similar behaviour is observed for the bump case, as shown in figure 4 (b). As indicated by the deformation of the $U = const$ contours in the $x = 15$ plane, the streaks are weaker and much more localised in the spanwise direction. The spatial structure of the eigenvector is similar to the one recovered for the cylinder, showing a mushroom-shaped disturbance on top of the central low-speed streak, with maximum velocity values located in the zones of maximum base-flow shear. However, the spatial support of the mode is much more compact in the spanwise direction.
These locations seem to indicate that these unstable global modes might be linked to a streak instability similar to the one recovered for parallel optimal streaks in Ref.[10] and that the instability mechanism might be related to the transport of the base flow shear by the perturbation. It is noteworthy that, for parallel streaks, the primary instability is of sinuous type, whereas in the present case it is of varicose type. However, one must note that for thinner roughness elements (not presented here) similar sinuous instabilities have also been recovered. The present results also confirm that, for large roughness elements, varicose perturbations are the most dangerous ones, as also highlighted by a global transient growth analysis in Ref.[11].

(a) (b)

Fig. 3 Streamwise velocity component of the eigenvector of the most unstable mode obtained at $Re = 1000$ for the cylindrical roughness element (a) and the smooth one (b).

4 Conclusion

The flows past two roughness elements, a cylindrical and a cubic-cosine one, have been investigated. The cylindrical roughness element induces strong streaks which appear to be well sustained in the streamwise direction, whereas in the bump case the streaks are weaker and eventually fade away. In both cases, a global stability

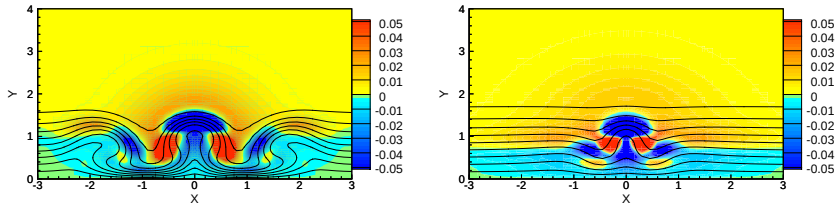

(a) (b)

Fig. 4 Shaded contours of the streamwise component the most unstable mode for the cylindrical roughness element in the plane $x = 25$ (a) and the cubic-cosine-shaped one at $x = 15$ (b) with $Re = 1000$. The solid lines are the base-flow streamwise velocity contours in the range $[0.1, 0.9]$.

analysis of the three-dimensional steady base flow has been carried out. In all of the cases considered, the spectra are composed by modes characterised by a varicose symmetry, mostly localised in the zones of large base flow shear and related to an instability of the quasi-parallel streaks. Finally, the critical Reynolds number being higher for the smooth bump than for the cylindrical roughness element might be related to the weaker amplitude of the induced streaks in the former case.

References

1. J.H.M. Fransson, A. Talamelli, L. Brandt, and C. Cossu. Delaying transition to turbulence by a passive mechanism . *Phys. Rev. Lett.*, 96(6):064501, 2006.
2. I. Tani, H. Komoda, Y. Komatsu, and M. Iuchi. Boundary-layer transition by isolated roughness . *Tech. Rep. 375*, 1962.
3. E. B. White. Transient growth of stationary disturbances in a flat plate boundary layer . *Phys. Fluids*, 14(12):4429, 2002.
4. M. Choudhari and P. Fischer. Roughness-induced transient growth. . *35th AIAA Fluid Dynamics Conference and Exhibit, Toronto, Ontario Canada*, AIAA-2005-4765, 2005.
5. A.E. von Doenhoff and A.L. Braslow. *The effect of distributed surface roughness on laminar flow and flow control*. Pergamon Press, Lachmann edition, 1961.
6. E. Akervik, L. Brandt, D. S. Henningson, J. Hoepffner, O. Marxen, and P. Schlatter. Steady solutions of the Navier-Stokes equations by selective frequency damping. *Phys. Fluids*, 18, 2006.
7. W. Edwards, L. Tuckerman, R. Friesner, and Sorensen D. Krylov methods for the incompressible Navier-Stokes equations . *J. Comput. Phys.*, 110(1):82–102, 1994.
8. S. Bagheri, E. Akervik, L. Brandt, and D. S. Henningson. Matrix-Free methods for the stability and control of boundary layer . *AIAA J.*, 47(5):1057–1068, 2009.
9. P. F. Fischer, J. W. Lottes, and S. G. Kerkemeier. Nek5000 Web page, 2008. http://nek5000.mcs.anl.gov.
10. P. Andersson, L. Brandt, A. Bottaro, and D. S. Henningson. On the breakdown of boundary layer streaks . *J. Fluid Mech.*, 428:29–60, 2001.
11. S. Cherubini, M. De Tullio, P. De Palma, and G. Pascazio. Transient growth in the flow past a three-dimensional smooth roughness element. *J. Fluid Mech.*, 724:642–670, 2013.